

Electronic Supporting information for manuscript
Chromium-Titanium nitride as efficient co-catalyst for photocatalytic
hydrogen production

Xiangjian Meng ^{a,b}, Weiliang Qi ^{a,b}, Wandi Kuang ^{a,b}, Samira Adimi ^{a,b}, Haichuan Guo ^{a,b}, Tiju Thomas ^d, Siqi Liu ^{*a,b}, Zhenping Wang ^{c*}, and Minghui Yang ^{*a,b}

^a *Ningbo Institute of Materials Technology & Engineering, Chinese Academy of Sciences, Ningbo, 315201, China*

^b *Center of Materials Science and Optoelectronics Engineering, University of Chinese Academy of Sciences, Beijing 100049, China*

^c *School of Chemical Engineering and Technology, Hebei University of Technology, Tianjin 300130, China*

^d *Department of Metallurgical and Materials Engineering, and DST Solar Energy Harnessing Center, Indian Institute of Technology Madras, Adyar, Chennai 600036, Tamil Nadu, India.*

* Correspondence Author: Dr. Siqi Liu; E-mail: liusiqi@nimte.ac.cn

* Correspondence Author: Prof. Minghui Yang; E-mail: myang@nimte.ac.cn

* Correspondence Author: Prof. Zhenping Wang; E-mail: wangzp@hebut.edu.cn

Table of Contents

I. Experimental Procedures

1. Computational methodology and model Detail.

II. Supplementary illustrations and explanations

Figure S1. XRD patterns of TiN, Cr_{0.5}Ti_{0.5}N and CrN.

Figure S2. EIS Nyquist plots of the sample (a) CrN and Cr₂O₃; (b) TiN and TiO₂.

Figure S3. DRS of (a)CrN, Cr₂O₃, (b)TiN, TiO₂ and (c)CrN, TiN, and Cr_{0.5}Ti_{0.5}N.

Figure S4. SEM images of pure (a) TiN, (b) CrN, and (c) Cr_{0.5}Ti_{0.5}N; TEM images of pure (d) TiN, (e) CrN, and (f) Cr_{0.5}Ti_{0.5}N (the inset image is statistic histogram of diameters).

Figure S5. (a) The HRTEM image of TiN; (b-c) HAADF-STEM image and the element mapping images of Ti, N.

Figure S6. (a) The HRTEM image of CrN; (b-c) HAADF-STEM image and the element mapping images of Cr, N.

Figure S7. XPS survey spectra of TiN, Cr_{0.5}Ti_{0.5}N, and CrN.

Figure S8. TEM images of (a,b) CdS NWs and (c,d) CdS-N NWs..

Figure S9. Zeta potential of functionalized TMNs and blank CdS NWs.

Figure S10. XRD patterns of CdS and CdS-N NWs.

Figure S11. SEM images of (a) CdS NWs; (b) CrN-5-CdS; (c) TiN-10-CdS and (d) Cr_{0.5}Ti_{0.5}N-12-CdS.

Figure S12. XRD patterns of (a) CrN-x-CdS; (b) TiN-x-CdS; (c) Cr_{0.5}Ti_{0.5}N-x-CdS.

Figure S13. UV-vis DRS of (a) CrN-x-CdS; (b) TiN-x-CdS and (c) Cr_{0.5}Ti_{0.5}N-x-CdS.

Figure S14. Photocatalytic H₂ evolution rates for (a) CrN-x-CdS; (b) TiN-x-CdS and (c) Cr_{0.5}Ti_{0.5}N-x-CdS.

Figure S15. Time resolved hydrogen evolution amount of (a) CrN-x-CdS; (b) TiN-x-CdS; (c) Cr_{0.5}Ti_{0.5}N-x-CdS and Pt-1-CdS.

Figure S16. (a) Photocatalytic H₂ evolution rate and (b) time-resolved hydrogen evolution amount of CdS and CdS-N NWs.

Figure S17. Photocatalytic HER rate over EY-sensitized CrN, TiN, and Cr_{0.5}Ti_{0.5}N.

Figure S18 Cycling tests of Cr_{0.5}Ti_{0.5}N-12-CdS composite over a period of 24 h.

Figure S19. XRD patterns and SEM of Cr_{0.5}Ti_{0.5}N-12-CdS nanocomposite before and after the photocatalytic reaction.

Figure S20. Transient I-t curves of CrN-(3-8)-CdS, Cr_{0.5}Ti_{0.5}N-(10-15)-CdS, and TiN-(8-10)-CdS without bias potential.

Figure S21. EIS Nyquist plots of CrN, TiN, and Cr_{0.5}Ti_{0.5}N.

Figure S22. Cyclic voltamogram curves of (a) CrN, (b) Cr_{0.5}Ti_{0.5}N, and (c) TiN in the double layer capacitive region at the scan rates of from 10 mV to 90 mV.

Scheme 1 Proposed mechanism for the photocatalytic H₂ generation of the CdS NWs (a) ad 1D TMN-CdS nanocomposites (b) under visible light irradiation with lactic acid as the sacrificial agent.

Table S1. XPS data for evaluation of the valence states of Ti, Cr, and N and the content of metal-N on the surface of TMN nanocomposites co-catalysts.

Table S2. Comparison of hydrogen production ratio for Cr_{0.5}Ti_{0.5}N-CdS with the ever-reported metal nitrides and carbides-based photocatalysts.

III. Supplementary References

I. Experimental Procedures

1. Computational Methodology and Model Detail.

The optimized stable structure and electronic characteristic calculations are conducted based on Density Functional Theory (DFT) implemented in quantum Espresso Package¹ in a plane wave basis, with the ultrasoft pseudo-potentials for electron-core interactions. The atomic valence electrons configurations are 2s² 2p³ for N, 3d² 3p⁶ 4s¹ 3d⁵ and 3s² 3p⁶ 4s² 3d² for Cr and Ti, respectively. Variable cell optimization was performed using Broyden, Fletcher, Goldfarb, and Shannon (BFGS) algorithm². We used our experimental results for the starting point and then the structures were fully relaxed until the residual forces on each atom is less than 10⁻³ eV. In wave vector K space, plane wave cut-off energy is considered 55 Ry in all calculations and we used a 6×6×6 k-point mesh, generated by the Monkhorste Pack method³.

II. Supplementary illustrations and explanations

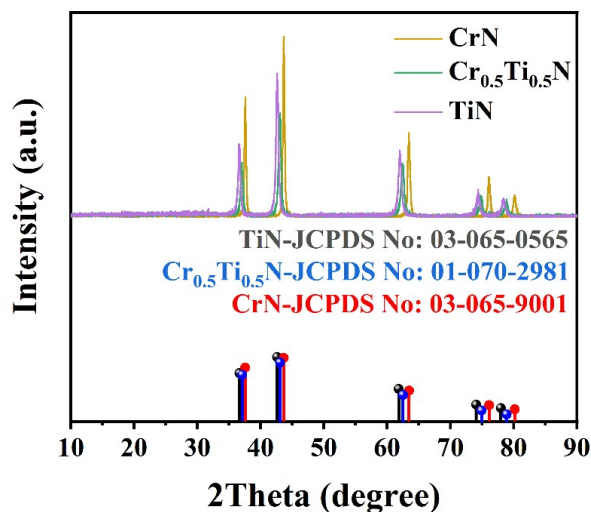


Fig. S1. XRD patterns of TiN, $\text{Cr}_{0.5}\text{Ti}_{0.5}\text{N}$ and CrN.

Note: The refined lattice parameters of TiN, $\text{Cr}_{0.5}\text{Ti}_{0.5}\text{N}$ and CrN are 4.2349(6) Å, 4.2079(7) Å and 4.1515(3) Å, respectively, which also indicates the large difference among the three specimens.

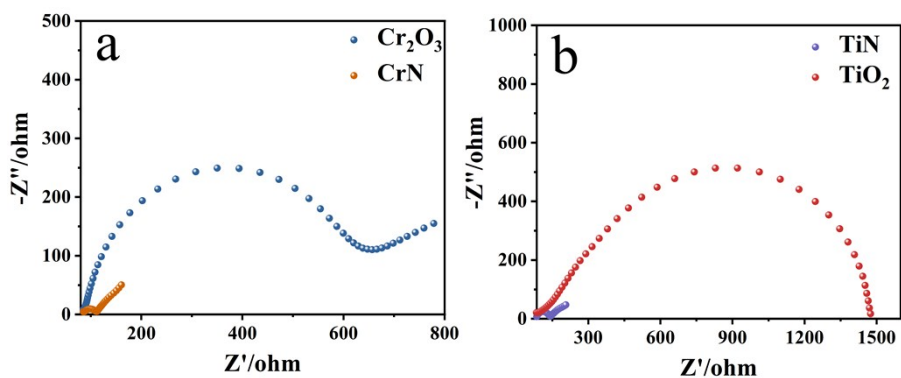


Fig. S2. EIS Nyquist plots of the sample (a) CrN- Cr_2O_3 ; (b) TiN- TiO_2 .

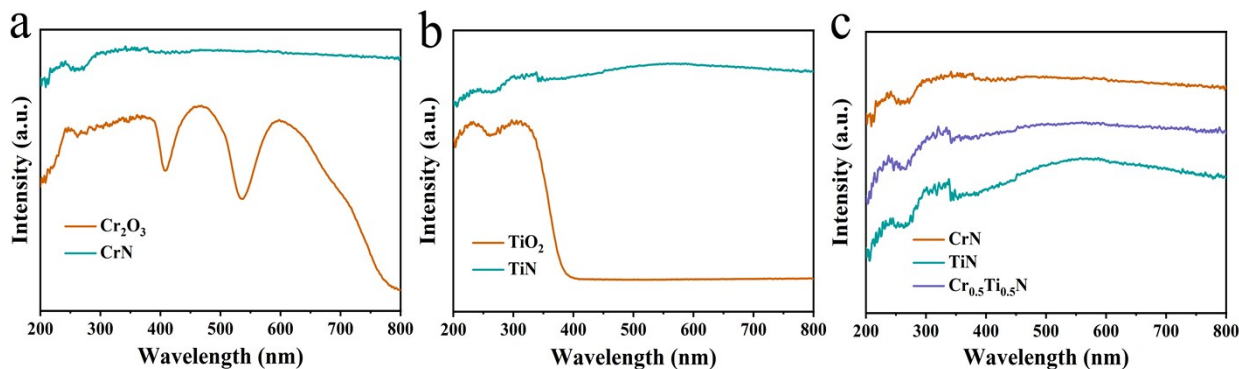


Fig. S3. DRS of (a)CrN, Cr_2O_3 , (b)TiN, TiO_2 and (c) $\text{Cr}_{0.5}\text{Ti}_{0.5}\text{N}$.

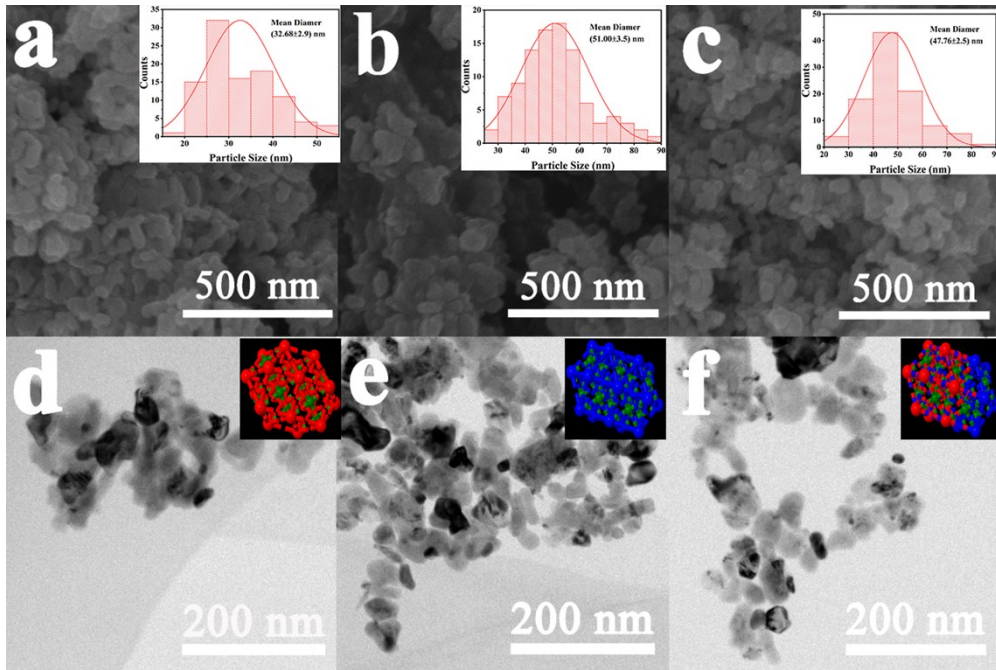


Fig. S4. SEM images of pure (a) TiN, (b) CrN, and (c) Cr_{0.5}Ti_{0.5}N (the inset image is statistic histogram of diameters); TEM images of pure (d) TiN, (e) CrN, and (f) Cr_{0.5}Ti_{0.5}N.

Note: The nitride product TMNs sample displays the morphology of small nanoparticle and their average particle size are respectively 32.7 nm (TiN), 51 nm (CrN), and 47.8 nm (Cr_{0.5}Ti_{0.5}N) in the inset image of Fig. S4.

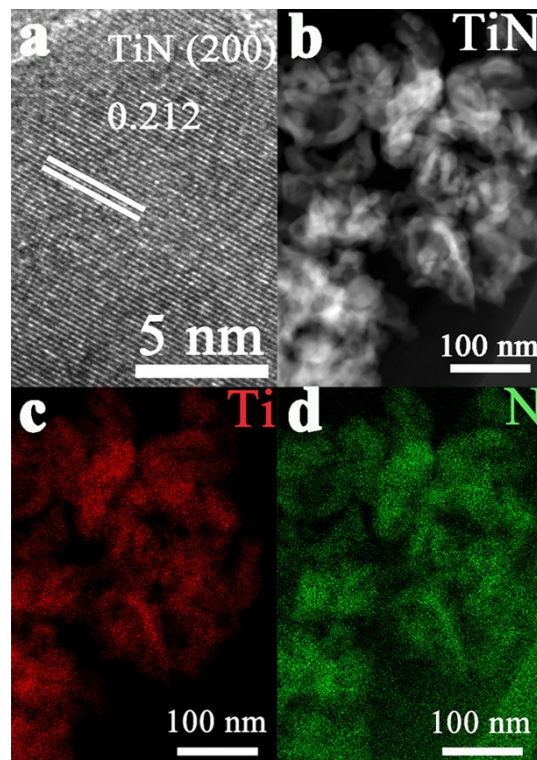


Fig. S5. (a) The HRTEM image of TiN; (b-c) HAADF-STEM image and the element mapping images of Ti, N.

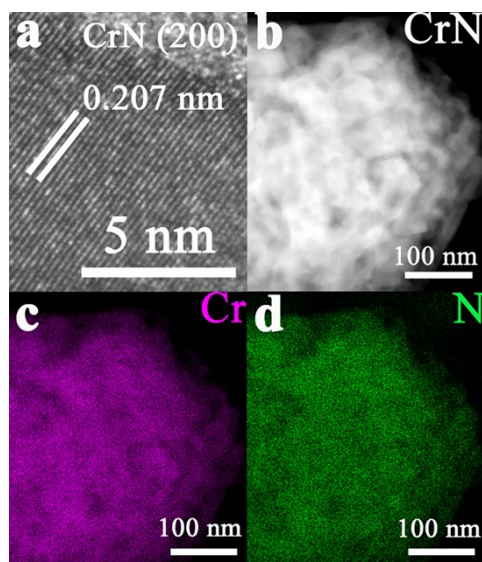


Fig. S6. (a) The HRTEM image of CrN; (b-c) HAADF-STEM image and the element mapping images of Cr, N.

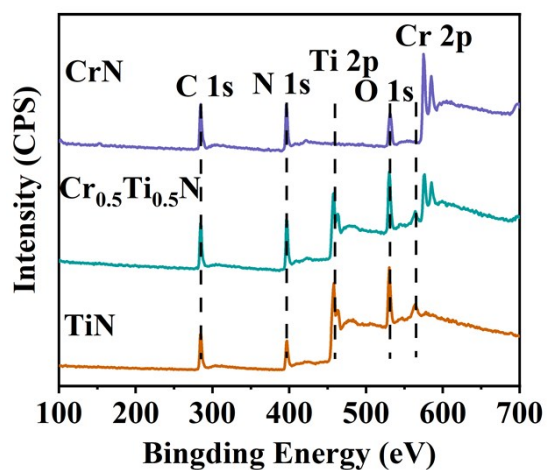


Fig. S7. (a) XPS survey spectra of TiN, $\text{Cr}_{0.5}\text{Ti}_{0.5}\text{N}$, and CrN.

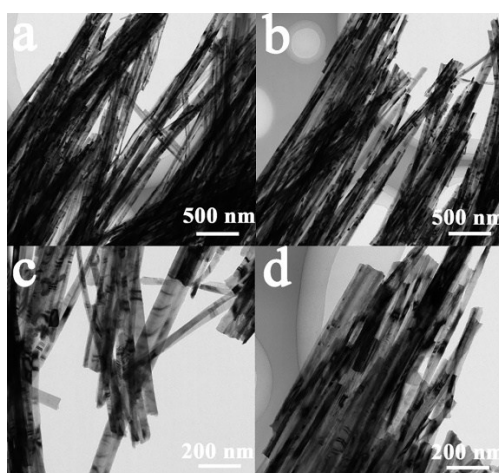


Fig. S8 TEM images of (a,c) CdS NWs and (b,d) CdS-N NWs.

Note: CdS-N NWs are the samples of NH_3 treated CdS nanowires.

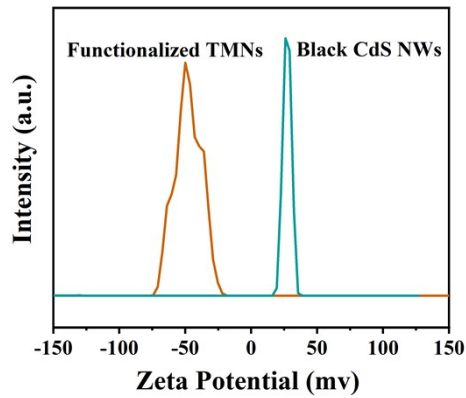


Fig. S9. Zeta potential of functionalized TMNs and blank CdS NWs.

Note: As shown in Fig. S9, after functionalized with SDS, the Zeta potential of TMNs is changed from positive to negative. Whereas, the Zeta potential analysis on CdS NWs reveals a positively charged surface of CdS. Thus, it is reasonable that the negatively charged SDS-functionalized TMNs and positively charged CdS NWs can spontaneously establish a solid basis of electrostatic attraction for the self-assembly construction of TMNs-CdS composites.

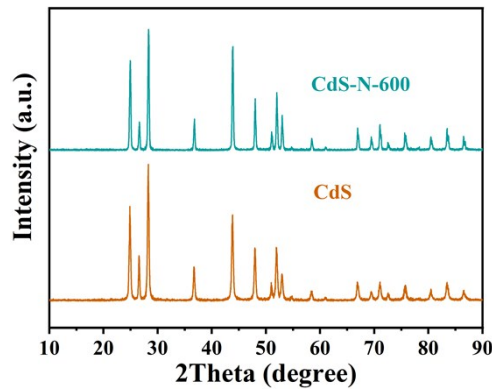


Fig. S10. XRD patterns of CdS and CdS-N NWs.

Note: CdS-N NWs are the samples of NH_3 treated CdS nanowires.

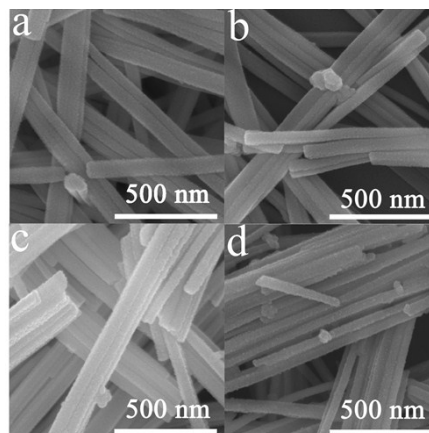


Fig. S11. SEM images of (a) CdS NWs; (b) CrN-5-CdS; (c) TiN-10-CdS and (d) Cr_{0.5}Ti_{0.5}N-12-CdS.

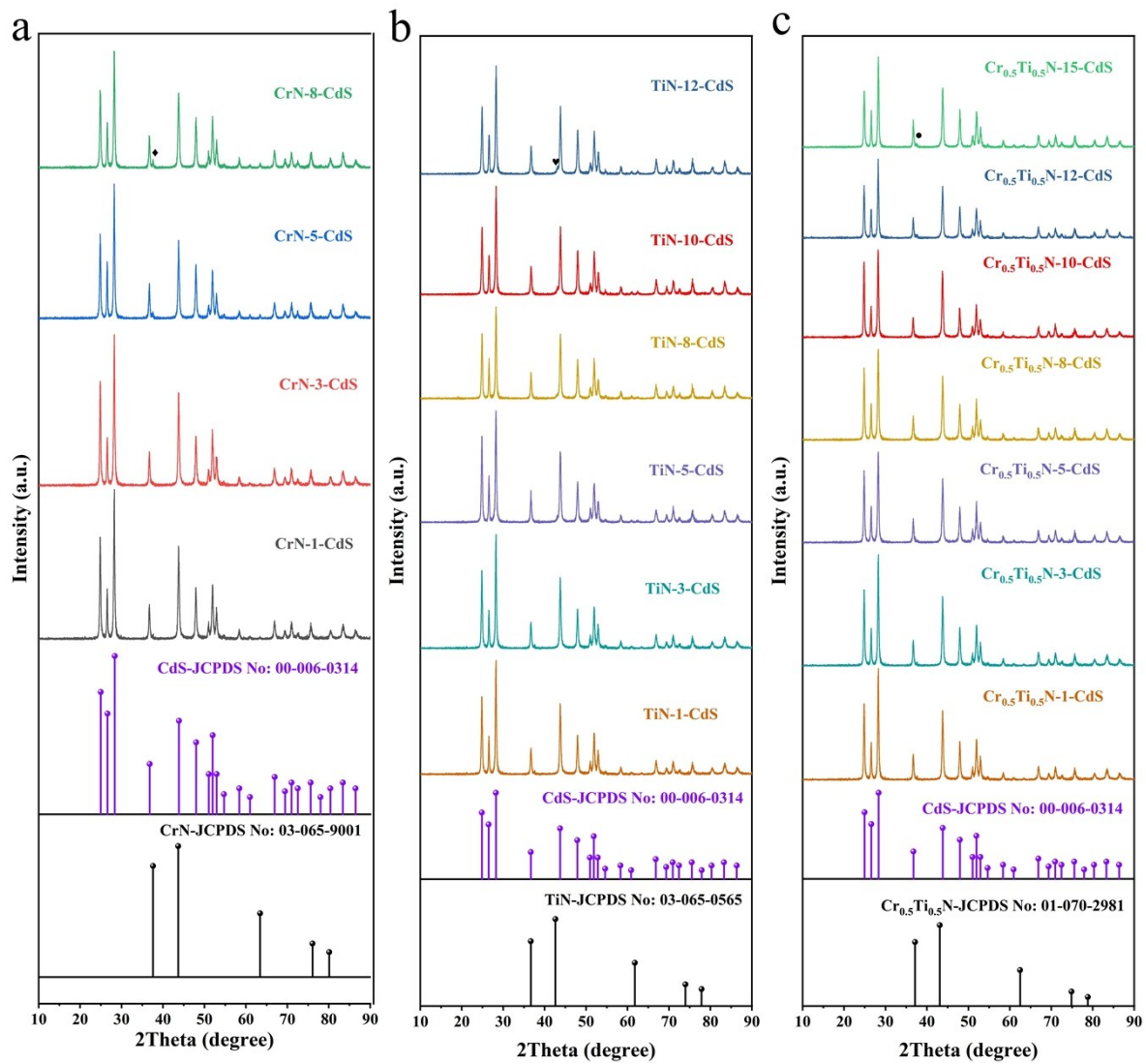


Fig. S12. XRD patterns of (a) CrN-x-CdS; (b) TiN-x-CdS; (c) Cr_{0.5}Ti_{0.5}N-x-CdS.

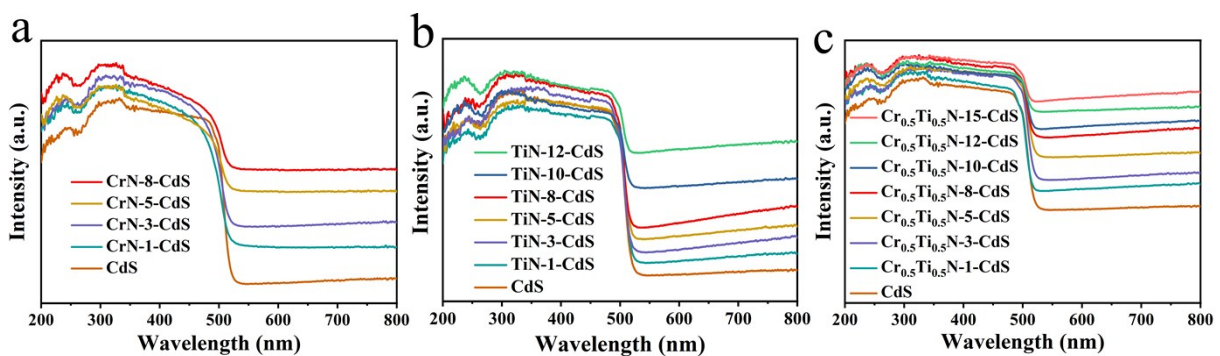


Fig. S13. UV-vis DRS of (a) CrN-x-CdS; (b) TiN-x-CdS and (c) Cr_{0.5}Ti_{0.5}N-x-CdS.

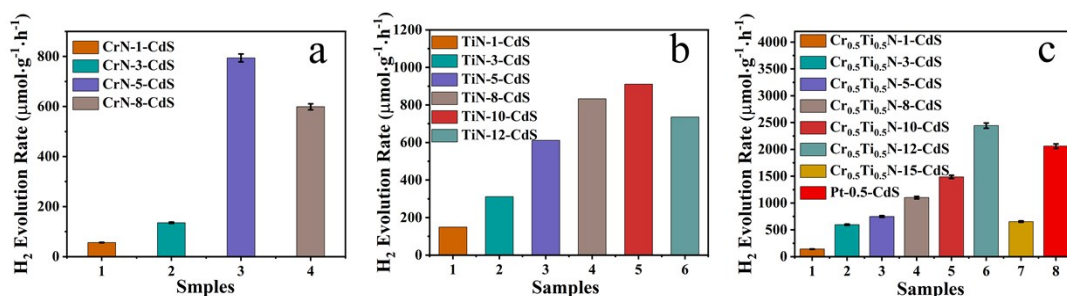


Fig. S14. Photocatalytic H₂ evolution rates for (a) CrN-x-CdS; (b) TiN-x-CdS and (c) Cr_{0.5}Ti_{0.5}N-x-CdS.

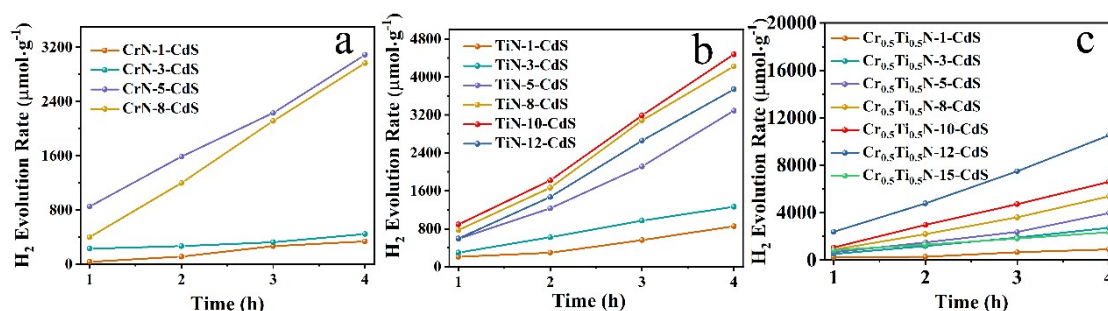


Fig. S15. Time-resolved hydrogen evolution amount of (a) CrN-x-CdS; (b) TiN-x-CdS; (c) Cr_{0.5}Ti_{0.5}N-x-CdS and Pt-1-CdS.

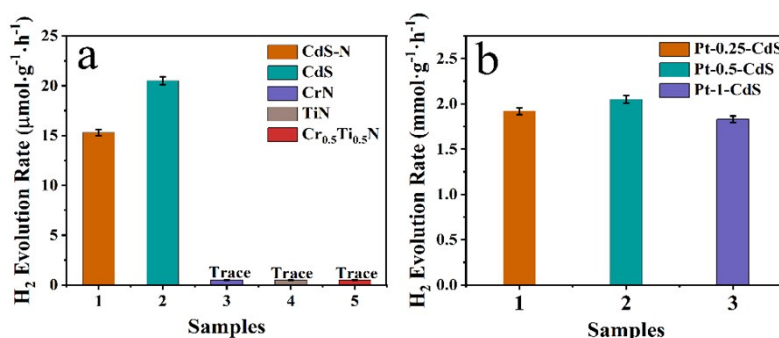


Fig. S16. (a) The photocatalytic H₂ evolution rate of CdS and CdS-N NWs, (b) Photocatalytic H₂ evolution rate of Pt-x-CdS NWs.

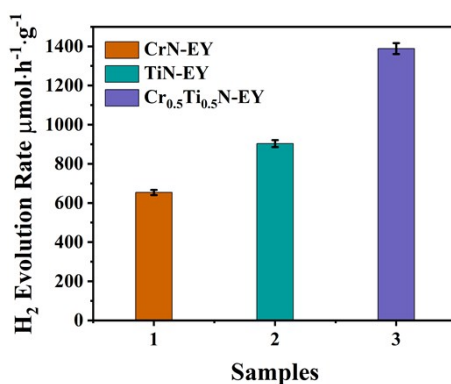


Fig. S17. Photocatalytic HER rate over EY-sensitized CrN, TiN, and Cr_{0.5}Ti_{0.5}N

Note: Typically, 10 mg of the prepared catalyst and 20 mg of Eosin Y were dispersed in 80

mL of a 10% (v/v) triethanolamine-water (TEOA-H₂O) solution by ultrasonication for 15 min.

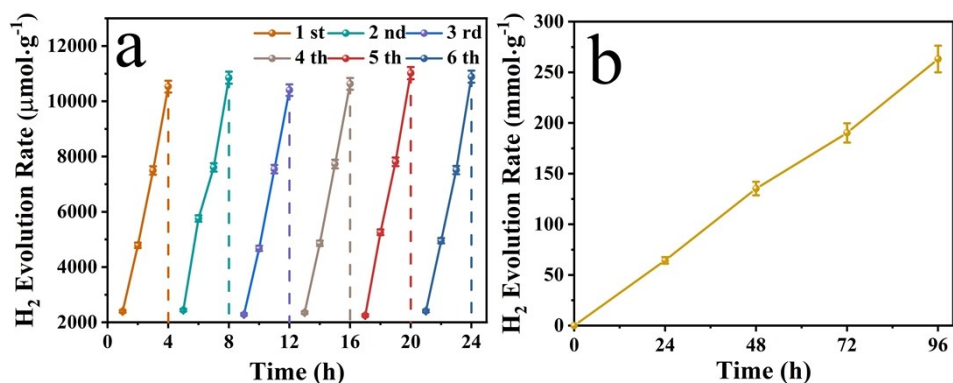


Fig. S18. (a) Cycling tests of Cr_{0.5}Ti_{0.5}N-12-CdS composite over a period of 24 h, and (b) long-term online tests of Cr_{0.5}Ti_{0.5}N-12-CdS composite over a period of 96 h.

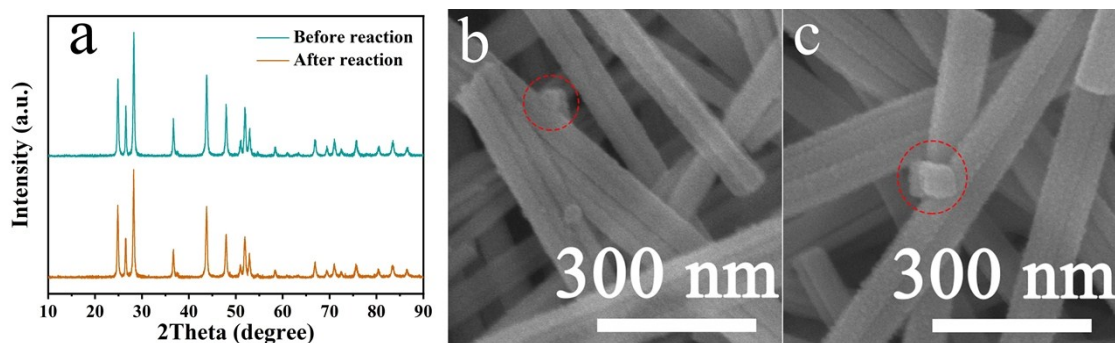


Fig. S19. (a) XRD patterns, (b-c) SEM of Cr_{0.5}Ti_{0.5}N-12-CdS nanocomposite before and after the photocatalytic reaction.

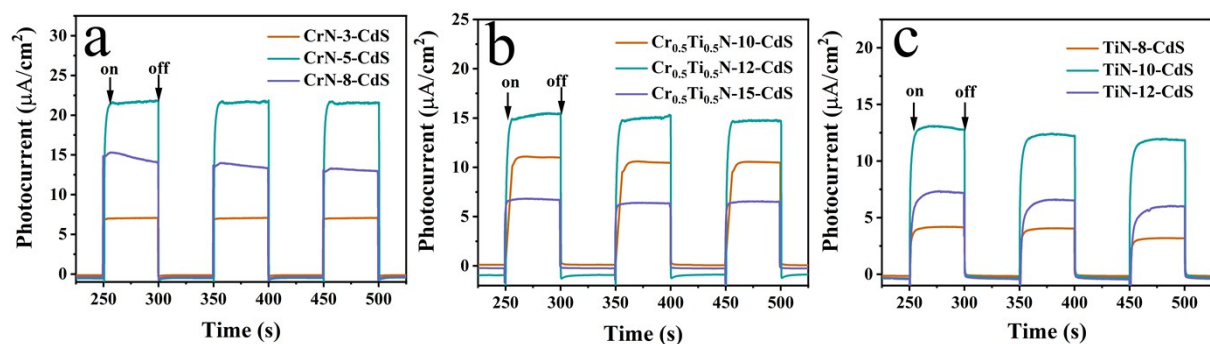


Fig. S20 Transient I-t curves of CrN-(3-8)-CdS, Cr_{0.5}Ti_{0.5}N-(10-15)-CdS, and TiN-(8-10)-CdS without bias potential.

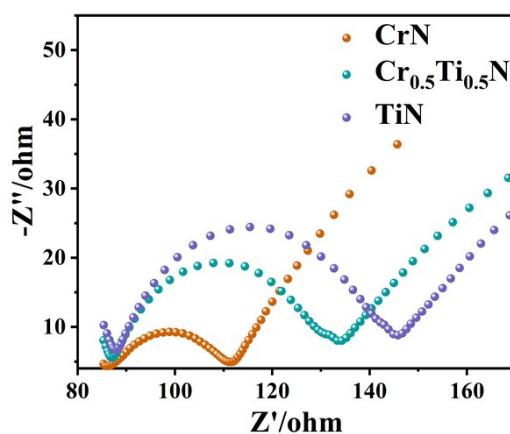


Fig. S21. EIS Nyquist plots of CrN, TiN, and $\text{Cr}_{0.5}\text{Ti}_{0.5}\text{N}$.

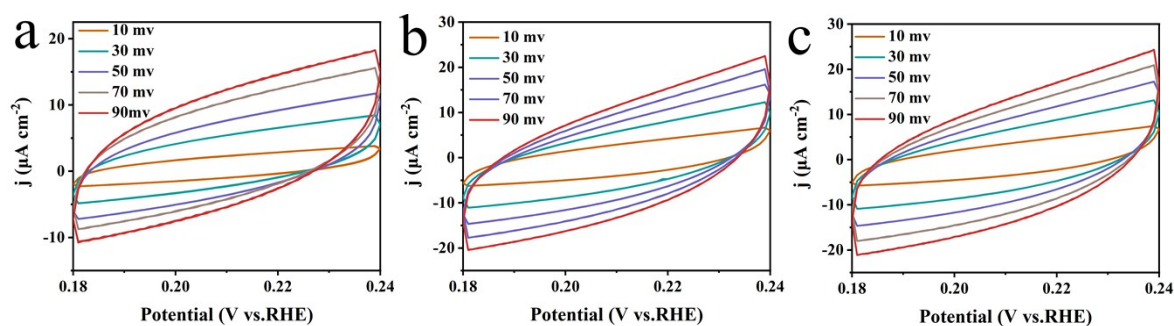
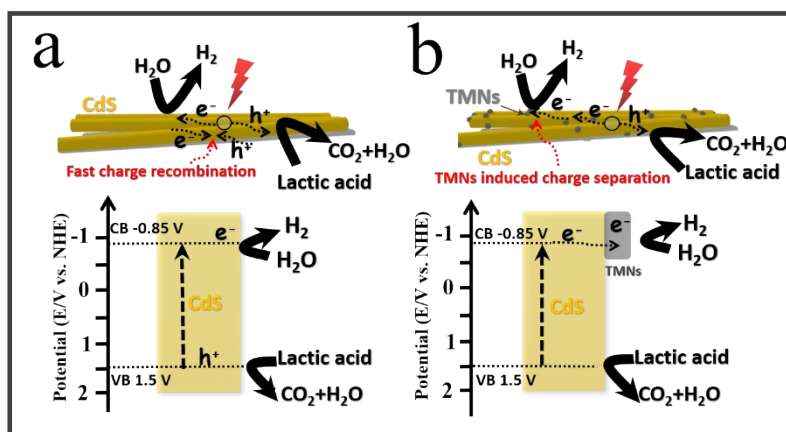


Fig. S22. Cyclic voltamogram curves of (a) CrN, (b) $\text{Cr}_{0.5}\text{Ti}_{0.5}\text{N}$, and (c) TiN in the double layer capacitive region at the scan rates of from 10 mV to 90 mV.



Scheme 1 Proposed mechanism for the photocatalytic H_2 generation of the CdS NWs (a) and 1D TMN-CdS nanocomposites (b) under visible light irradiation with lactic acid as the sacrificial agent.

Table S1. XPS data for evaluation of the valence states of Ti, Cr, and N and the content of metal-N on the surface of TMN nanocomposites co-catalysts.

Cocatalyst	Ti 2p _{3/2} (eV) and Area (%)	BE shift	Cr 2p _{3/2} (eV) and Area (%)	BE shift	N1s (eV)	Metal-N (at%)
TiN	Ti-N 455.6 (11.94%)				Ti-N 396.8	21.2%
	Ti-O 458.5 (40.13%)					
	Ti-O-N 456.95 (47.93%)				N-H 399.1	
Cr _{0.5} Ti _{0.5} N	Ti-N 455.88 (31.38%)	+0.28 eV	Cr-N 575.66 (57.46%)	+0.24 eV	Cr/Ti-N 396.9	23.87%
	Ti-O 458.5 (44.82%)	0				
	Ti-O-N 456.72 (23.8%)	-0.23 eV	Cr-O-N 577.1 (42.54%)	-0.25 eV	N-H 399.1	
CrN			Cr-N 575.42 (72.66%)		Cr-N 396.6	20.28%
			Cr-O-N 576.85 (27.34)		N-H 399.1	

Note: As shown in Table 2, the high-resolution Ti 2p spectra for Cr_{0.5}Ti_{0.5}N and TiN samples. For the high-resolution Ti 2p spectrum of the TiN, the peaks located at 455.6 eV (2p_{3/2}) and 461.32 eV (2p_{1/2}) are in accordance with a metallic state of Ti while peaks of 456.72 eV (2p_{3/2}) and 462.07 eV (2p_{1/2}) are assigned to the Ti-O-N bonds in TiN sample. The peaks of 485.5 eV (2p_{3/2}) revealed the existence of Ti-O, suggesting an oxidized surface which is easily obtained in TMNs materials. Similarly, Cr_{0.5}Ti_{0.5}N also shows three couples of peaks corresponding metallic state of Ti (455.88 eV for Ti 2p_{3/2} and 461.04 eV for 2p_{1/2}), Ti-O-N bonds (456.95 eV for Ti 2p_{3/2} and 462.07 eV for 2p_{1/2}) and Ti-O bonds (485.5 eV for Ti 2p_{3/2}), respectively. Notably, over 0.2 eV of Ti 2p spectra for Cr_{0.5}Ti_{0.5}N as compared to that of TiN are observed. This result reveals the reduced electron density of the Ti (TiN Ti) atoms in Ti-N and increased electron density of the Ti atoms in Ti-O-N over Cr_{0.5}Ti_{0.5}N after grafting. As mirrored in Fig. 2c, the peaks at 575.42 eV (CrN-Cr 2p_{3/2}) and 575.66 eV (Cr_{0.5}Ti_{0.5}N-Cr 2p_{3/2}) reveal the existence of Cr-N bonds, while the other two peaks at 577.1 eV (CrN-Cr 2p_{3/2}) and 576.85 eV (Cr_{0.5}Ti_{0.5}N-Cr 2p_{3/2}) are related to Cr-O-N.⁴⁶ Clearly, the Cr 2p_{3/2} and Cr 2p_{1/2} peaks of Cr-N in the Cr_{0.5}Ti_{0.5}N cocatalyst are shifted about 0.2 eV toward higher binding energy, which indicates the reduction in electron density. Meanwhile, the peaks of Cr-O-N are shifted toward the opposite direction, which reveals that the electron density of the Cr (Cr-O-N) atoms increasing after grafting. These XPS peak shifts could be attributed to the changes of TiN and CrN chemical states in ternary nitride Cr_{0.5}Ti_{0.5}N.

Table S2. Comparison of hydrogen production ratio for Cr_{0.5}Ti_{0.5}N-CdS with the ever-reported metal nitrides and carbides-based photocatalysts.

Cocatalyst	Photocatalyst	Light source	Reaction solution	^a PHER rate	Ref.
Cr _{0.5} Ti _{0.5} N	CdS	300 W Xe, 420 ≥nm	10 v% lactic acid	120	This work
Ni ₃ N	CdS	300 W Xe, 420 ≥nm	0.25 M Na ₂ S/0.35 M Na ₂ SO ₃	10	[1]
Co ₃ N	CdS	300 W Xe, 420 ≥nm	0.75 M Na ₂ S/1.05 M Na ₂ SO ₃	6.5	[2]
InN	TiO ₂	300 W Xe, 420 ≥nm	rhodamine B (RhB, 2.5 × 10 ⁻⁵ mol L ⁻¹).	45	[3]
TiN	TiO ₂	300 W Xe, UV-Vis, 420 ≥nm	10 v% methanol (CH ₃ OH)	UV-Vis 19; Vis 1.3	[4]
MoC (QDs)/Carbon Film	ZnIn ₂ S ₄	300 W Xe, 400 ≥nm	10 v% lactic acid	4.8	[5]
Mo ₂ C@C	CdS	300 W Xe, 420 ≥nm	10 v% lactic acid	25.7	[6]
Ni ₃ C	CdS	350 W Xe, 420 ≥nm	0.25 mol L ⁻¹ of Na ₂ S–Na ₂ SO ₃	7.7	[7]

Note: ^aPHER rate denotes the hydrogen evolution rate of times higher than pristine photocatalyst.

III. Supplementary References:

- [1] P. Giannozzi, S. Baroni, N. Bonini, M. Calandra, R. Car, C. Cavazzoni, D. Ceresoli, G. L. Chiarotti, M. Cococcioni, I. Dabo, *J Phys Condens Matter*. **2009**, *21*, 395502.
- [2] J. D. Head, M. C. Zerner, *Chem Phys Lett*. **1985**, *122*, 264-270.
- [3] J. P. Perdew, K. Burke, M. Ernzerhof, *Phys Rev Lett*. **1996**, *77*, 3865-3868.
- [4] Z. Sun, H. Chen, L. Zhang, D. Lu, P. Du, *J. Mater. Chem. A*. **2016**, *4*, 13289-13295.
- [5] H. Chen, D. Jiang, Z. Sun, R. M. Irfan, L. Zhang, P. Du, *Catal. Sci. Technol*. **2017**, *7*, 1515-1522.
- [6] Z. Su, H. Li, P. Chen, S. Hu, Y. Yan, *Catal. Sci. Technol*. **2017**, *7*, 5105-5112.
- [7] X. Yu, Z. Zhao, D. Sun, N. Ren, L. Ding, R. Yang, Y. Ji, L. Li, H. Liu, *Chem Commun*. **2018**, *54*, 6056-6059.
- [8] F. Gao, Y. Zhao, L. Zhang, B. Wang, Y. Wang, X. Huang, K. Wang, W. Feng, P. Liu, *J. Mater. Chem. A*. **2018**, *6*, 18979-18986.
- [9] Y.-X. Pan, J.-B. Peng, S. Xin, Y. You, Y.-L. Men, F. Zhang, M.-Y. Duan, Y. Cui, Z.-Q. Sun, J. Song, *ACS Sustain. Chem. Eng*. **2017**, *5*, 5449-5456.
- [10] M. Song, Y. Deng, J. Xie, K. He, L. Wei, X. Chen, L. Xin, *Appl Catal B Environ*. **2018**, *227*, 218-228.